Journal of Applied Polymer Science

Pressure-Crystallized Piezoelectric Structures in Binary Fullerene C70/Poly(vinylidene fluoride) Based Composites

Daopeng Zhang,[1,2] Pengfei Tian,[1] Xin Chen,[1] Jun Lu,[1,3] Rui Huang[4]

[1]Key Laboratory of Advanced Technologies of Materials, Ministry of Education, School of Materials Science and Engineering, Southwest Jiaotong University, Chengdu 610031, Sichuan, China

[2]Xi'an Yongdian Electric Co., Ltd, Xi'an 710016, Shaanxi, China

[3]State Key Laboratory of Molecular Engineering of Polymers, Fudan University, Shanghai 200433, China

[4]College of Polymer Materials Science and Engineering, Sichuan University, Chengdu 610065, Sichuan, China

Correspondence to: J. Lu (E-mail: junluprc@hotmail.com)

ABSTRACT: The effective fabrication of polar crystalline structures of poly (vinylidene fluoride) (PVDF), such as beta and gamma, is crucial to the development of piezoelectric polymer devices. In this study, we report the effect of pressure on binary fullerene C70/PVDF-based composite with an overall good C70 dispersion, which was prepared by an easy physical and mechanical route. The C70/PVDF composites were crystallized in a piston-cylinder high-pressure apparatus, and the polymeric crystalline structures totally with extended-chain piezoelectric beta- or gamma-form lamellae were successfully achieved in the composite samples by varying temperature, pressure, crystallization time, and composite composition. The *c*-axis thickness of the extended-chain beta-form lamellae of PVDF in the composites increased and decreased with the increase of the applied temperature and pressure, respectively, and it increased with the increase of crystallization time. Although C70 was found to be negative for the rapid formation of beta-form PVDF crystals, it played an important role in the growth of a beta-form PVDF nanowire with extended-chain crystalline substructures. The template-free formation of such piezoelectric nanowires was attributed to a C70-induced self-assembly of the polymer, driven by physical interactions at high pressure. The pressure-crystallized C70/PVDF composites, self-reinforced with unique one-dimensional piezoelectric structures, may diversify niche applications in advanced functional polymeric devices. © 2013 Wiley Periodicals, Inc. J. Appl. Polym. Sci. 130: 1823–1833, 2013

KEYWORDS: composites; morphology; nanotubes; graphene and fullerenes; phase behavior

Received 26 January 2013; accepted 8 April 2013; Published online 6 May 2013

DOI: 10.1002/app.39377

INTRODUCTION

Since the mass production of fullerenes has become possible,[1] fullerene/polymer composites have attracted considerable attention from the materials research community. The combination of fullerenes with polymers makes it possible to create novel materials that exhibit the unique properties of fullerenes while taking advantages of the easy processability of polymers.[2,3] Incorporating fullerene C60 or its derivatives into a polymer matrix was already been shown to be an effective route for improving its photovoltaic, electromechanical, and thermomechanical properties significantly.[4–6] Another higher fullerene, C70, appears to be the next most likely candidate for rapid experimental progress in fullerene family, though its outstanding properties are still not widely employed in polymers at present stage.[7–9]

Huang et al.[10] reported the synthesis of C70 chemically modified poly (*N*-vinylcarbazole) (PVK) through direct reaction of carbanion intermediates of PVK with C70. The resultant polymer was highly soluble in some common organic solvents, and the thermal stability of pure PVK was apparently enhanced by C70 chemical modification. Higuchi et al.[11] succeeded in obtaining homogeneous fullerene (a mixture of C60 and C70)-dispersed polystyrene membranes having a diameter of more than 90 mm using the casting method under reduced pressure. The permeability coefficients of pure nitrogen, oxygen, carbon dioxide, ethane, and ethylene were found to increase significantly in the fullerene membranes compared to those in the polystyrene membranes. The permeability increase was thought to be originated from the increase in diffusion coefficients in the fullerene membranes. Aseyev et al.[12] studied aqueous solutions of poly (vinyl pyrrolidone) (PVP)-fullerene C70 complexes using static and dynamic light scattering, and observed two diffusion process. The slow diffusion described the motion of large PVP/C70 clusters, while the fast diffusion was associated

with the presence of single PVP molecules or small individual PVP/C70 complexes with the order of a single PVP chain. Zuev et al.[13] examined the effect of the fulleroid fillers (fullerene C60, mixture of C60/C70, and fulleroid soot) on mechanical, tribological, and electrical properties of the nanocomposites based on polyamide-6 (PA6), which were prepared by in situ polymerization. The mechanical properties of composites were improved by the introduction of fullerenes and fullerene soot, and the friction coefficient for the nanocomposites with fulleroid fillers was practically two times lower than that of the neat PA6. The reinforcement effect of fullerenes was attributed to a fullerene-induced selective crystallization, which resulted in only the alpha-form crystals in the polymer matrix.

Particularly, recent investigations showed that the fullerene C70 was suitable to replace fullerene C60 as electron transporter and acceptor in polymer solar cells (PSCs).[14–16] Li et al. [14] studied the effect of the additives of 3-methylthiophene (MT) and 3-hexylthiophene (HT) on the photovoltaic performance of the devices, in order to further improve the power conversion efficiency (PCE) of the poly (3-hexylthiophene) (P3HT)/indene-C70 bisadduct (IC70BA)-based PSCs. The PCE of the PSCs was improved from 5.80% for the device without the additive to 6.35% for the device with HT additive and to 6.69% with MT additive. With the MT or HT processing additive, the active layer of the blend of P3HT/IC70BA showed strengthened absorbance, enhanced crystallinity, and improved film morphology. They also presented PSCs with P3HT as a donor, an IC70BA as an acceptor, a layer of indium tin oxide modified by MoO_3 as a positive electrode, and Ca/Al as a negative electrode.[15] The optimized PSCs exhibited a high PCE of 6.68%, and the excellent performance was attributed to the higher crystallinity of P3HT and a better donor–acceptor interpenetrating network of the active layer prepared under the optimized conditions. Moreover, a new soluble C70 derivative, dihydronaphthyl-based C70 bisadduct (NC70BA), was synthesized and explored as acceptor in PSCs,[16] and the PSC based on the blend of P3HT and NC70BA showed a high open-circuit voltage and a high PCE. The amorphous nature of NC70BA effectively suppressed the thermally driven crystallization, which led to high thermal stability of the P3HT:NC70BA-based solar cell devices.

Poly (vinylidene fluoride) (PVDF) and its copolymers with trifluoroethylene are one of the limited known piezoelectric class of polymers. They promise applicability in diverse field of technology due to their high piezoelectric activity and availability as flexible thin films.[17–21] As for PVDF, it exhibits a pronounced polymorphism, i.e., α, β, γ, δ, and ε, transforming between several crystal forms under certain conditions.[22,23] The successful development of ferroelectric polymer devices depends on the effective fabrication of polar ferroelectric crystalline structures, such as β and γ.[17–20]

The introduction of organic or inorganic fillers, especially those with size in nanoscale, was already tried by the researchers for controlling the crystal phase and morphology of the polymer.[24–26] However, to the best of our knowledge, the physical or chemical interactions between PVDF and fullerene C70 have not been reported yet. Particularly, no investigation was performed on C70/PVDF composite at high pressure.

In fact, solid phase forming under high pressure is a more effective route to produce polymer products with greatly improved physical and mechanical properties. This is achieved by creating the desired crystal morphologies with ideal molecular orientation during the processing.[27] Therefore, the investigations on polymer crystallization at high pressure may reveal more structures, morphologies and properties instructive to the high-pressure processing of polymers.[28]

For PVDF, pressure treatment has been proved to be an effective route to enhance the yielding of its β- or γ-form crystals.[29,30] Also, fullerenes and their derivatives were found to be promising materials in promoting the formation of new polymeric structures at high pressure.[6,31,32] In this study, we report for the first time the effect of pressure on binary fullerene C70/PVDF-based composite with an overall good C70 dispersion. The polymeric crystalline structures totally with extended-chain piezoelectric β- or γ-form lamellae were successfully achieved in the composite samples by varying temperature, pressure, crystallization time, and composite composition. Furthermore, the introduction of C70 into the polymer matrix resulted in the unexpected growth of a β-form PVDF nanowire with extended-chain crystalline substructures.

EXPERIMENTAL

Materials

C70 powder (>99.0 wt/wt purity) was purchased from Puyang Yongxin Fullerene Co. and used as received. PVDF powder, commercial-grade Solef 6010, was supplied by Solvay Co., Shanghai. The corresponding weight-average molecular weight, M_w, was 322,000 g/mol. C70 and PVDF were pre-mixed at 23,000 rpm, room temperature for 10 min in a commercial Joyoung JYL-C012 blender. This was followed by melt compounding at 60 rpm and 210°C for 15 min using a torque rheometer (ZJL-300, Changchun Intelligent Instrument Company, Changchun, China). The as-prepared C70/PVDF binary composites were pelletized subsequently by using a smashing machine (FW400A, Beijing Zhongxingweiye Instrument Co., Beijing, China) for high-pressure experiments. Before melt blending and high-pressure treatment, the starting materials (C70 and PVDF) were held at 80°C in vacuum for 12 h to eliminate moisture.

Sample Preparation

High-pressure experiments for the as-prepared C70/PVDF composites were carried out with a self-made piston-cylinder high-pressure apparatus.[32] The following procedure for crystallization was used. After loading the samples, the temperature was increased to a level (200°C) to allow them to be melted. Then low pressure (150–200 MPa) was applied, and the temperature was raised to a predetermined level. After equilibrium was established, the pressure was further raised to the predetermined level. These samples were kept under these conditions for a pre-determined time, and then quenched down to ambient condition. This procedure ensured the minimum degradation of PVDF at elevated temperature, and the polymer would be in a molten state before crystallization took place.

Characterization

Transmission electron microscopy (TEM) detections were performed with a Tecnai G^2 F20 S-TWIN apparatus (FEI), employing

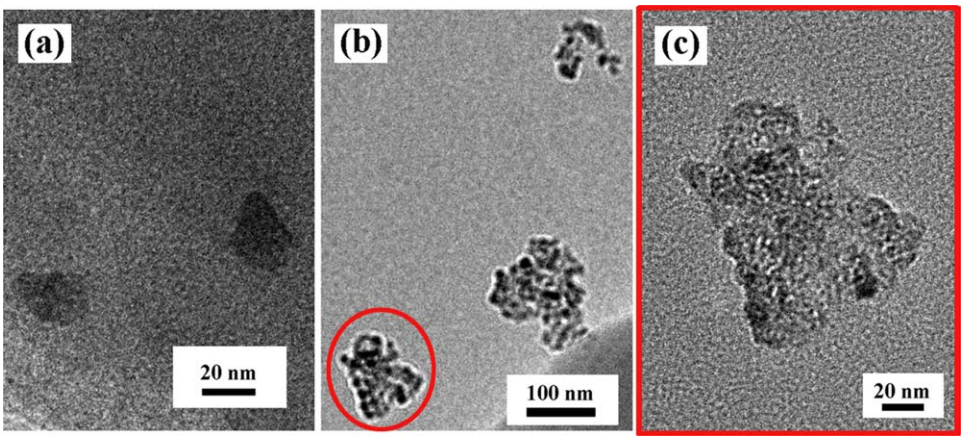

Figure 1. TEM photographs of the C70/PVDF composite samples with (a) 0.5 wt % and (b) 1.0 wt % C70 loadings, respectively. c is the magnified view of the portion highlighted by an elliptical frame in b. [Color figure can be viewed in the online issue, which is available at wileyonlinelibrary.com.]

a Leica EMUC6/FC6 microtome for the preparation of ultrathin sections through room-temperature microtomy. Differential scanning calorimetry (DSC) measurements were conducted at atmospheric pressure by using a TA-Q20 instrument (TA Instruments). The weight of sample was around 5 mg. The melting behavior of the crystals was investigated through a heating scan with a heating rate of 10°C/min at N_2 atmosphere. Wide-angle X-ray diffraction (WAXD) results were obtained at room temperature with a PANalytical X'pert PRO diffractometer (PANalytical BV, Almelo, The Netherlands). Attenuated total reflectance Fourier transform infrared spectroscopy (ATR-FTIR) data were obtained using a Nicolet 5700 spectrometer (Thermo Electron Scientific Instruments) in the range of 700–4000 cm^{-1}, with 32 scans conducted at a resolution of 4 cm^{-1}. WAXD and ATR-FTIR data were collected at the fresh and smooth surfaces of the samples, which were obtained through fracture at liquid N_2 temperature. After the WAXD and ATR-FTIR characterizations, the sample surfaces were etched by using a method modified from that developed by Vaughan,[33] and then coated with gold for scanning electron microscopy (SEM) observations using a HITACHI S-3400 apparatus (Hitachi, Tokyo, Japan).

RESULTS AND DISCUSSION

Figure 1 shows the TEM results of the as-fabricated C70/PVDF composite samples before the applied treatment by pressure. As can be seen, an overall good dispersion of C70 nano-aggregations in PVDF matrix was achieved. The average size of the C70 agglomerations increased with the increase of C70 loading levels. Also, a close examination on the morphology of the C70 aggregations showed that they were actually organized by still smaller C70 nano particles [Figure 1(c)].

The C70/PVDF composite with 1.0 wt % C70 loading was selected for the high pressure experiments by varying temperature, pressure, and crystallization time. The crystallization conditions, as well as the results of DSC, WAXD, and ATR-FTIR, are shown in Figures 2–4. Figure 2(a) displays the DSC results of the C70/PVDF composite samples crystallized at 500 MPa and different maximum quenching temperature. The results revealed that generally the melting temperatures of the high-pressure treated composite samples increased with the increase of crystallization temperature. Two melting points were detected for both the samples crystallized at 230 and 245°C maximum quenching temperature, respectively. When the maximum quenching temperature was further increased to 260°C, the low-temperature peak shifted to a higher temperature, and a shoulder was formed on the low-temperature side of the main high temperature peak. Finally, a single whole melting peak was observed on the DSC curve of the sample crystallized at 280°C. The melting points of the sample crystallized at 260 and 280°C reached 201.78 and 203.91°C, respectively, which are more than 20°C higher than those of the sample crystallized at 230°C. The DSC data indicated that crystal form transforming occurred with the crystallization temperature increase.[29,30] Furthermore, the higher melting points for the samples respectively crystallized at 260 and 280°C suggested that a greater perfection for the crystals of PVDF was obtained, which may possibly be assigned to the formation of extended-chain crystals with β or γ form.[29,30]

Commonly, the identification of the crystalline phases of PVDF was carried out by WAXD and FTIR measurements. Referring to the X-ray diffraction data,[29,30,34] the reflections of monoclinic α phase of the polymer at 2θ angles 17.7, 18.5, 19.9, and 26.5° are attributed to planes (100), (020), (110), and (021), respectively. The apparent single peak of orthorhombic β phase at 20.4–21.1° actually comes from the superposition of (110) and (200) reflections. The characteristic reflections of monoclinic γ phase are assigned to planes (020), (200), and (110), overlapped with 020α, 200β, and 110β, respectively.[35] For IR bands, they are characteristic of α phase at 764, 796, 976, and 1214 cm^{-1}, β phase at 840 and 1280 cm^{-1}, and γ phase at 840 and 1234 cm^{-1}, respectively.[36,37] The relevant WAXD and ATR-FTIR spectra of the composite samples crystallized at 500 MPa and variant maximum quenching temperature are shown in Figure 2(b,c), respectively. As can be observed, with the increase of crystallization temperature, the intensity of the peaks characteristic of α and β phase decreased and increased, respectively, whether in WAXD or IR spectra. The γ form crystals of PVDF

Applied Polymer SCIENCE

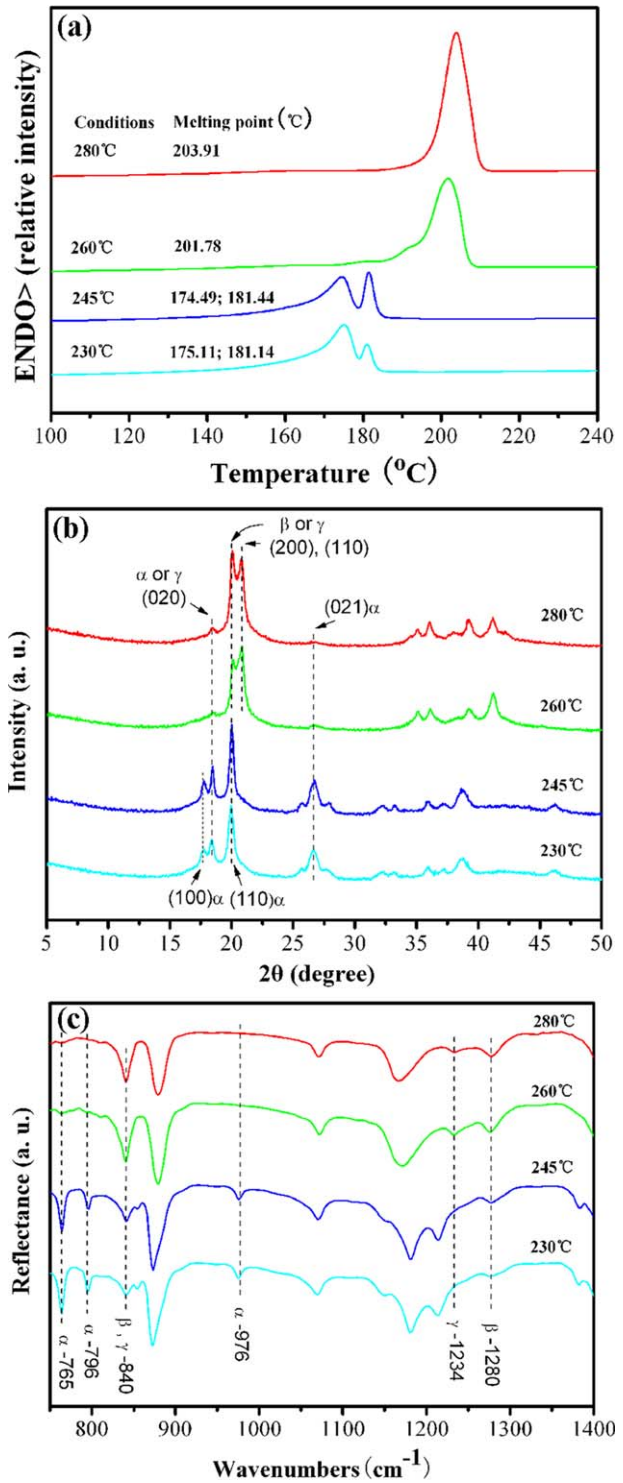

Figure 2. (a) DSC, (b) WAXD, and (c) ATR-FTIR results of the C70/PVDF (1/99, wt/wt) composite samples crystallized at 500 MPa and different maximum quenching temperature. [Color figure can be viewed in the online issue, which is available at wileyonlinelibrary.com.]

began to appear evidently when the crystallization temperature was reached to 260°C. However, their amount decreased drastically when the temperature was further increased to 280°C. Particularly, no α phase was detected in the samples crystallized at 260 and 280°C, respectively, and their crystal forms are totally a mixture of β and γ phase.

Figure 3(a) shows the DSC data of the C70/PVDF samples crystallized at 500 MPa, 260°C for different time. Only single endotherms emerged on the DSC curves of the composite samples

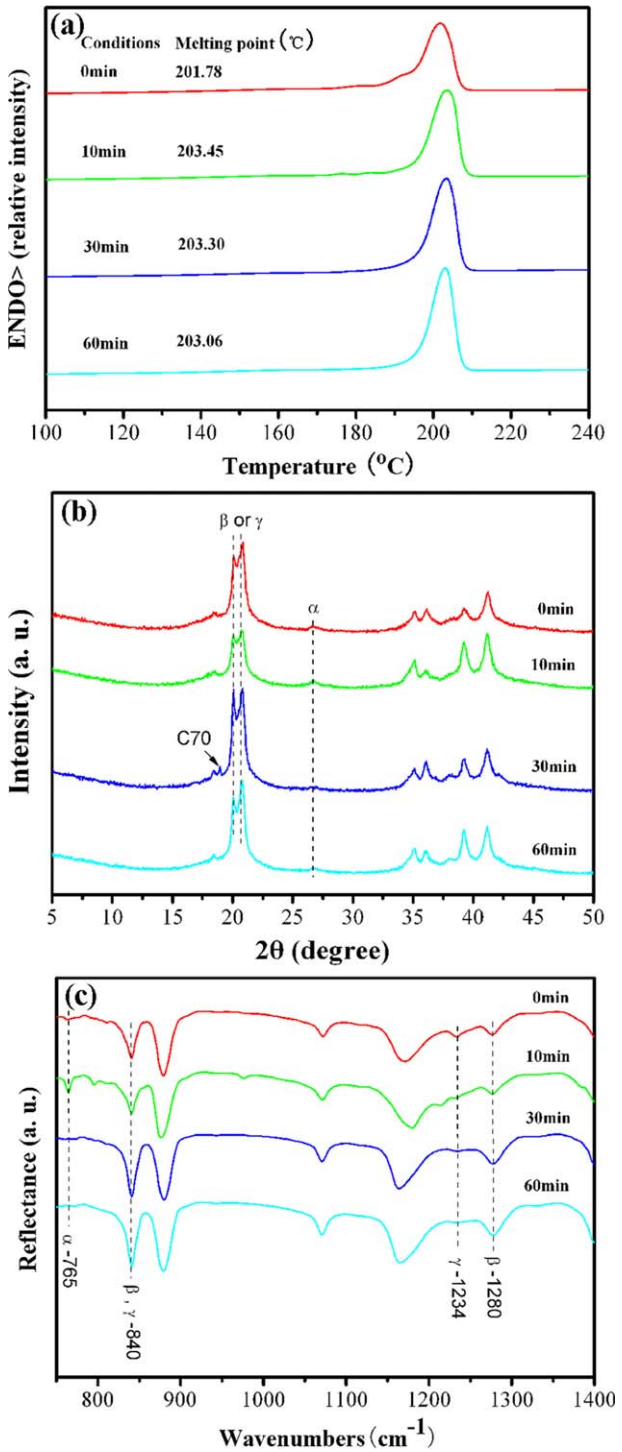

Figure 3. (a) DSC, (b) WAXD, and (c) ATR-FTIR results of the C70/PVDF (1/99, wt/wt) composite samples crystallized at 500 MPa, 260°C for different time. [Color figure can be viewed in the online issue, which is available at wileyonlinelibrary.com.]

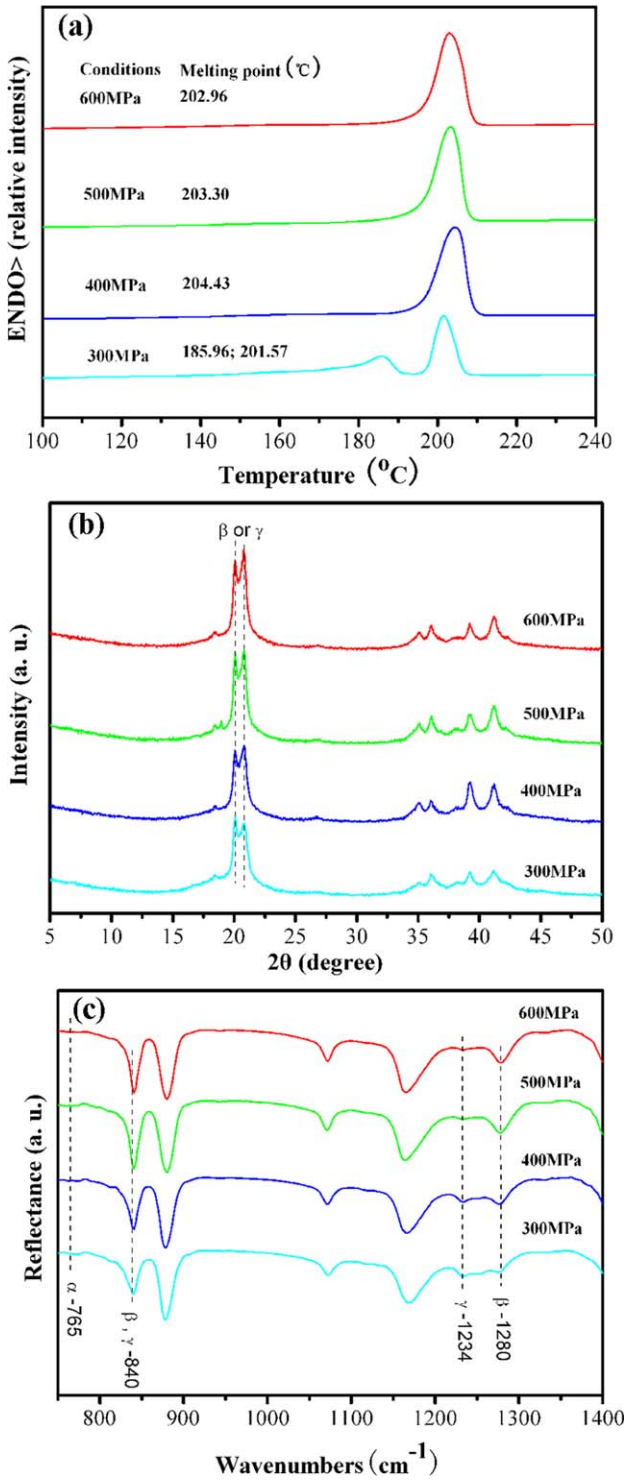

Figure 4. (a) DSC, (b) WAXD, and (c) ATR-FTIR results of the C70/PVDF (1/99, wt/wt) composite samples crystallized at different pressure, 260°C for 30 min. [Color figure can be viewed in the online issue, which is available at wileyonlinelibrary.com.]

crystallized during 0–60 min. The melting point increased with the increase of crystallization time within 10 min, and it remained more or less the same when crystallization time was further prolonged. The results showed that 10–30min was enough to crystallize a C70/PVDF composite sample with a high melting point, at the same applied pressure and temperature. Also, the 201–203°C melting points still suggested that PVDF crystals with extended-chain lamellae as substructures were crystallized in the composite samples of this group.[29,30]

Considering the characteristic bands of WAXD and IR shown in Figure 3(b,c), the reflection bands of α-phase appeared when crystallization time was increased to 10 min, though no such phase was detected for the sample crystallized at 500 MPa and 260°C maximum quenching temperature (0 min). Nevertheless, the bands characteristic of α-phase disappeared both in WAXD and IR spectra, if crystallization time was above 30 min. We also noted that the band intensity of β and γ phase increased and decreased all through the experimental time range, respectively. This suggested that the extended-chain crystals with β form were more stable than those with γ form, especially at high temperature and high pressure.

Figure 4 shows the characterization results for another group C70/PVDF composite samples, crystallized at different pressure, 260°C for 30 min. Two melting peaks appeared on the DSC curve of the sample crystallized at 300 MPa. The low (185.96°C) and high (201.57°C) endotherm regions should associate with the melting of two distinct populations of PVDF crystals, with folded- and extended-chain substructures, respectively.[29,30] When crystallization pressure was increased to 400 MPa, only single melting peak was observed, and the melting point was as high as 204.43°C. Further increasing pressure resulted in the slight decrease of the melting points. However, the melting points for the samples crystallized at 500 and 600 MPa, respectively, were still within the range of those for extended-chain crystals. The WAXD and IR bands in Figure 4(b,c) show no α-phase crystals. Combined with the above DSC data, they further confirmed that the polymeric crystalline structures in the composite samples were totally with piezoelectric β- or γ-form lamellae. The tendency of intensity change of the bands for β phase was just contrary to that for γ phase. The reflection intensity of β-phase increased with the increase of pressure, but that of γ phase decreased. This indicated that pressure increase might be more favorable for the formation of β-phase crystals. Moreover, the results in Figure 4 suggested that a composite sample with crystals of entire piezoelectric extended-chain structures could be obtained by the crystallization at appropriate pressure, on the condition that the crystallization time was long enough.

Figure 5 shows the ATR-FTIR spectra of the original PVDF sample, and the C70/PVDF composite samples with different C70 loadings. All the samples were prepared at 500 MPa, 260°C for just 10 min. The intensity of the bands characteristic of α phase increased, while that typical of β and γ phase decreased, along with the increase of the loading level of C70. This suggested that C70 might play a negative role in the rapid formation of both β- and γ-form PVDF crystals. However, as shown in Figure 3(c), all the α-form crystals, promoted by C70 within relative short time, were transformed into β-form crystals, if the crystallization time was further increased.

The above DSC, WAXD, and IR data were further confirmed by SEM observations.[38–40] For example, a large amount of featured

Applied Polymer SCIENCE

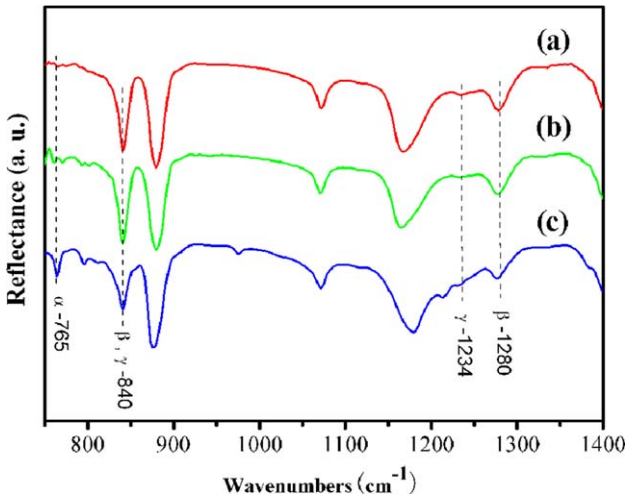

Figure 5. ATR-FTIR results of the (a) original PVDF and C70/PVDF composite samples with (b) 0.5 wt %, and (c) 1.0 wt % C70 loadings, respectively, crystallized at 500 MPa, 260°C for 10 min. [Color figure can be viewed in the online issue, which is available at wileyonlinelibrary.com.]

α spherulites were observed in the composite sample crystallized at 500 MPa and 245°C maximum quenching temperature [Figure 6(a)]. When the quenching temperature was increased to 260°C, the number of nano-structured crystallites corresponding to γ form increased, and almost no trace of α spherulites was detected. The typical morphology of such γ-form crystallites are shown in Figure 6(b).

Although DSC, WAXD, and IR results indicated that extended-chain crystals of PVDF, with β or γ form, were possibly obtained in certain samples, direct morphologies should be given with SEM measurements. Figure 7 shows the secondary electron images of the etched fracture surfaces of C70/PVDF (1/99, wt/wt) composite samples, crystallized at 500 MPa and different maximum quenching temperature. For the sample crystallized at 230°C, fiber-like structures of β crystallites were observed [Figure 7(a)]. The fibrils were randomly packed, and the relatively low melting points of the sample suggested that they were actually with folded-chain substructures. When crystallization temperature was increased to 260°C, oriented β-form fibrils with extended-chain lamellae as substructures were revealed, as shown in Figure 7(b). Particularly, Figure 7(c,d) gives out typical SEM photographs of the composite sample crystallized at 280°C, in which the striated appearance, the most characteristic feature for polymer extended-chain crystals, was exposed clearly. According to the previous investigations,[41,42] the striations of the β-form extended-chain crystals should run parallel to the molecular chains.

Figure 8 shows the typical morphology of the extended-chain crystals in the C70/PVDF (1/99, wt/wt) composite samples, crystallized at 500 MPa, 260°C for different time. With the increase of crystallization time, the *c*-axis thickness of the β-form extended-chain crystals increased. Especially, γ-form extended-chain crystals, grown together with β-form crystals, were also observed [Figure 8(a,b)], with their striations clearly exposed during the sample fracture. The thickness along *c* axis of the β-form crystals was around 4 and 6 μm when the sample was crystallized for 30 and 60 min, respectively [Figure 8(c,d)].

The morphological observation results from Figures 7 and 8 showed that, generally, the *c*-axis thickness of the extended-chain β-form lamellae in the composite samples increased with the increase of crystallization temperature and time. However, further morphological studies showed that it decreased with the increase of the applied pressure (Figure 9). For the C70/PVDF (1/99, wt/wt) composite samples crystallized at 600 MPa, 260°C for 30 min, almost no striated appearance was exposed for the β-form crystals, though the DSC data suggested that they are endowed with extended-chain substructures [Figure 9(a)]. Other conditions being the same, another sample was prepared at 400 MPa. In Figure 9(b), its fracture surface was covered with

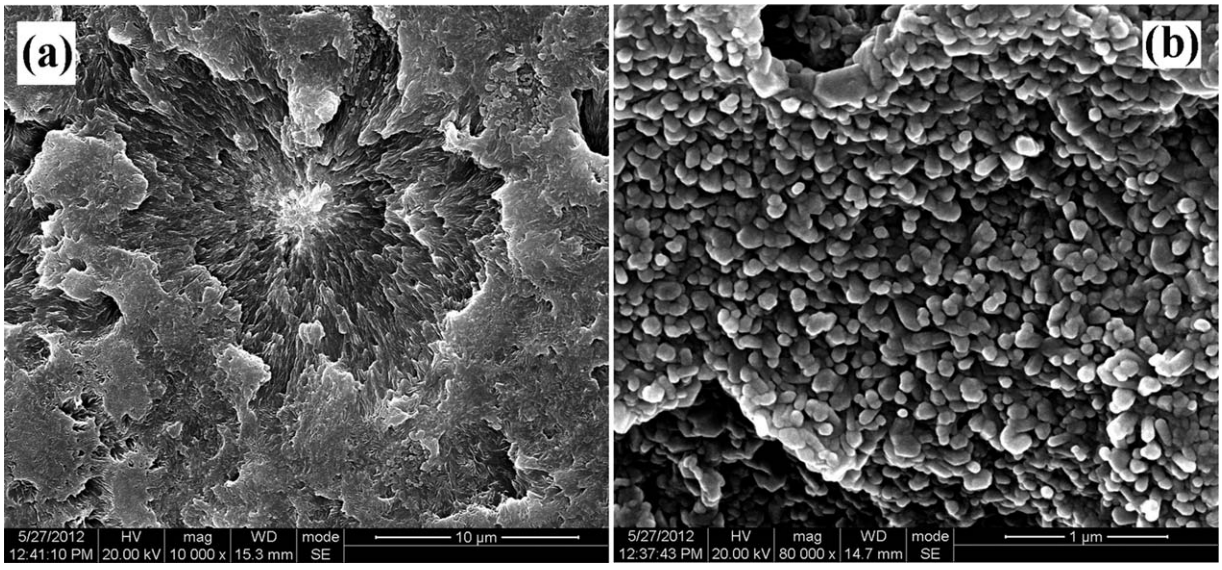

Figure 6. Secondary electron images of the etched fracture surfaces of C70/PVDF (1/99, wt/wt) composite samples, crystallized at 500 MPa and different maximum quenching temperature: (a) 245°C; (b) 260°C.

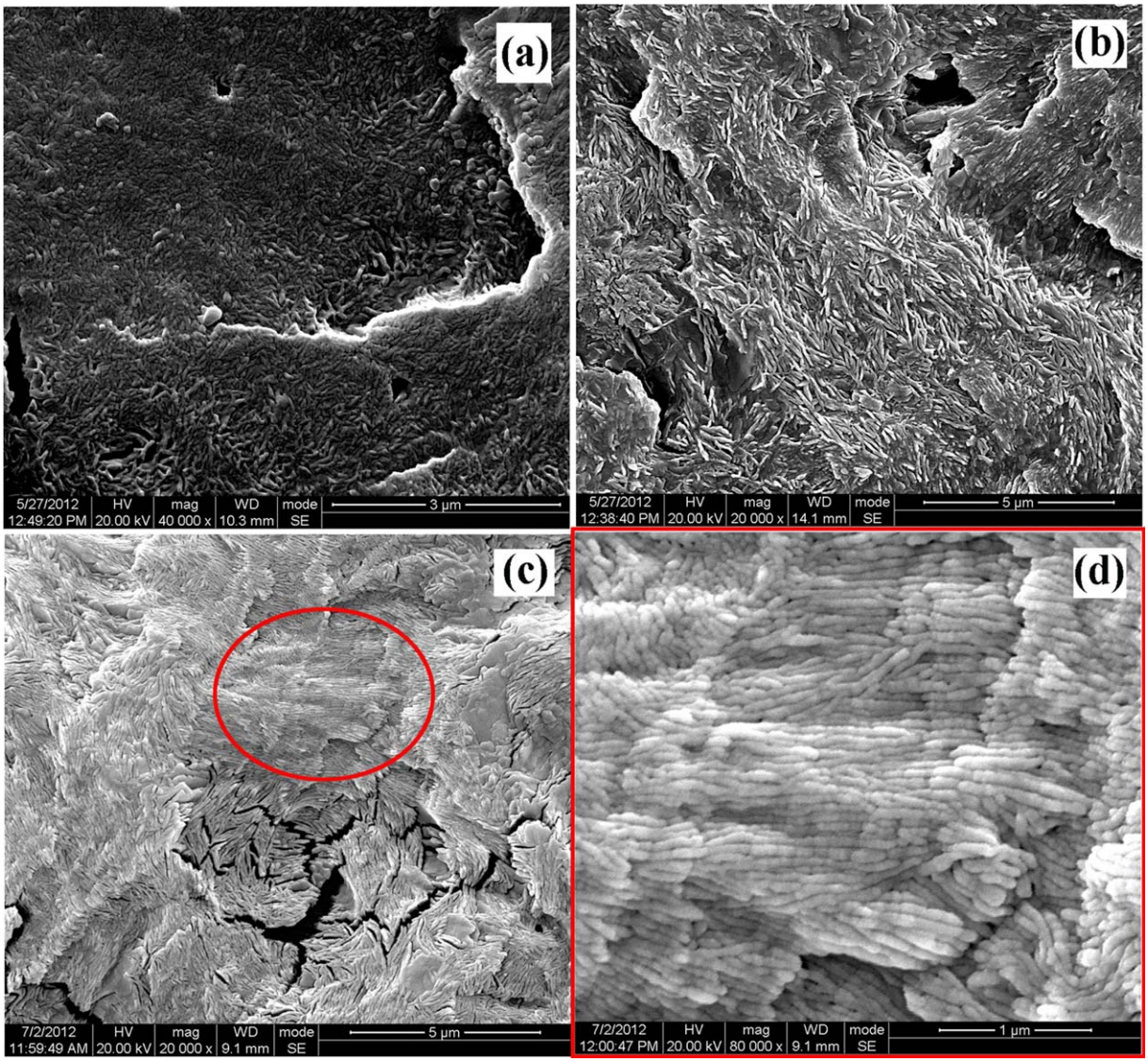

Figure 7. Secondary electron images of the etched fracture surfaces of C70/PVDF (1/99, wt/wt) composite samples, crystallized at 500 MPa and different maximum quenching temperature: (a) 230°C; (b) 260°C; (c,d) 280°C. d is the magnified view of the portion highlighted by an elliptical frame in c. [Color figure can be viewed in the online issue, which is available at wileyonlinelibrary.com.]

striated β-form extended-chain crystals. When the pressure was decreased to 300 MPa, the *c*-axis thickness of the β-form extended-chain crystals was around 7 μm for just 30 min crystallization [Figure 9(c)]. Moreover, γ-form extended-chain crystals were also observed in the same sample [Figure 9(d)].

Recently, we investigated the crystallization of well-dispersed fullerene C60/PVDF nano-composites at high pressure, and obtained crystalline β-form PVDF nanowire arrays by a template-free approach.[43] However, the relatively low melting points of the C60/PVDF composite samples indicated that the fabricated polymeric nanowires were with folded-chain substructures. Figure 10(a) shows another secondary electron image of the etched fracture surface of the C70/PVDF (1/99, wt/wt) sample crystallized at 500 MPa and 280°C maximum quenching temperature. As can be seen, nanowires with polygonal shape were also formed. The nanowires were observed only after the etching of the amorphous parts of the fracture surfaces. So they totally belong to a crystalline entity. As for the PVDF nanowires fabricated by a template method, commonly they were an amorphous and crystalline mixture.[44,45] Furthermore, the high melting point (203.91°C) of the C70/PVDF composite sample suggested that they were actually with extended-chain substructures, which was quite different from those crystallized in the C60/PVDF samples.[43] The size and morphology of PVDF nanowires in C70/PVDF composites were also sensitive to the crystallization conditions. For example, with the decrease of the applied pressure, generally, the diameters of the nanowires decreased, and their lengths increased [Figure 10(b,c)].

The collected WAXD and IR data were reexamined to identify the crystal form of the as-fabricated PVDF nanowires. For the

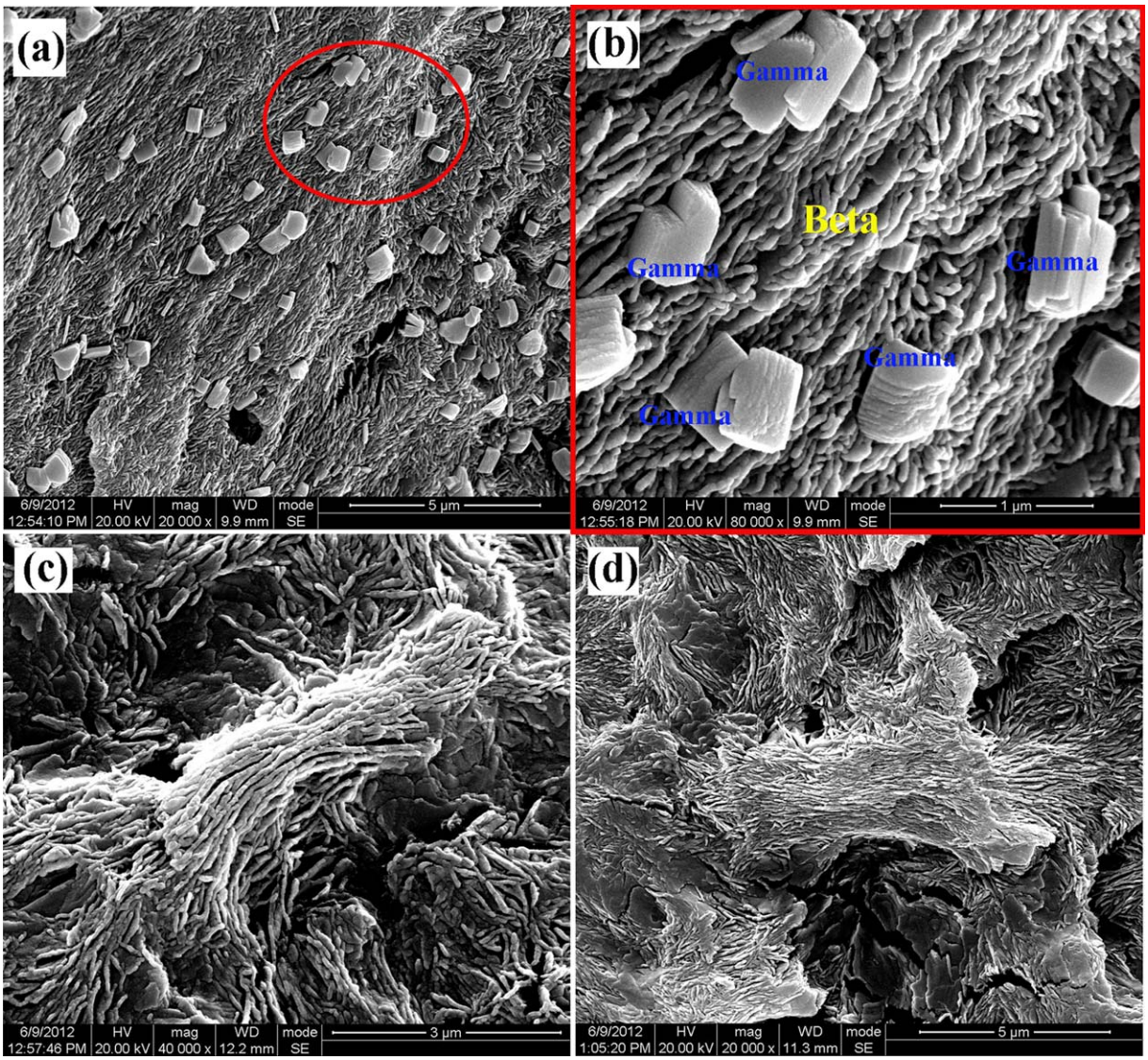

Figure 8. Secondary electron images of the etched fracture surfaces of C70/PVDF (1/99, wt/wt) composite samples, crystallized at 500 MPa, 260°C for different time: (a,b) 10 min; (c) 30 min; (d) 60 min. b is the magnified view of the portion highlighted by an elliptical frame in a. [Color figure can be viewed in the online issue, which is available at wileyonlinelibrary.com.]

sample crystallized at 500 MPa and 280°C maximum quenching temperature, which was totally a mixture of β and γ phase, a large numbers of nanowires were formed [Figure 2(b,c)]. Thus the existence of α phase can be excluded from such nanowires. Other conditions being the same, when the sample was crystallized at 260°C maximum quenching temperature, the intensity of the bands characteristic of γ phase increased drastically. Nevertheless, no nanowire was observed in the sample [Figure 2(b,c)]. So the formation of γ phase in the nanowires can be further excluded. Conclusively, the crystal form for the obtained PVDF nanowires in the C70/PVDF composite samples belong to crystalline β phase.

In the C70/PVDF composite sample with 0.5 wt % C70 loading, exactly crystallized at 500 MPa, 260°C for 10 min, the growth of nanowires was also observed, though their number was substantially decreased. No trace of nanowire formation was observed on the fracture surface of a pristine PVDF sample, crystallized under the same conditions, and etched with the same process. Therefore, it is concluded that C70 plays an important role in the growth of the PVDF nanowires. Furthermore, although β-form crystalline nanowires with extended-chain substructures were formed in certain pressure-crystallized C70/PVDF samples, unlike those in their C70/PVDF counterparts, the nanowires did not form the expected arrays at the above experimental conditions.

The growth of PVDF nanowires may be attributed to a C70-induced self-assembly at high pressure.[43] Self-assembly driven by physical or chemical interaction has been proved to be an effective route to construct nanoscale materials with a one-dimensional structure.[46–51] Also, it is known that the sensitivity

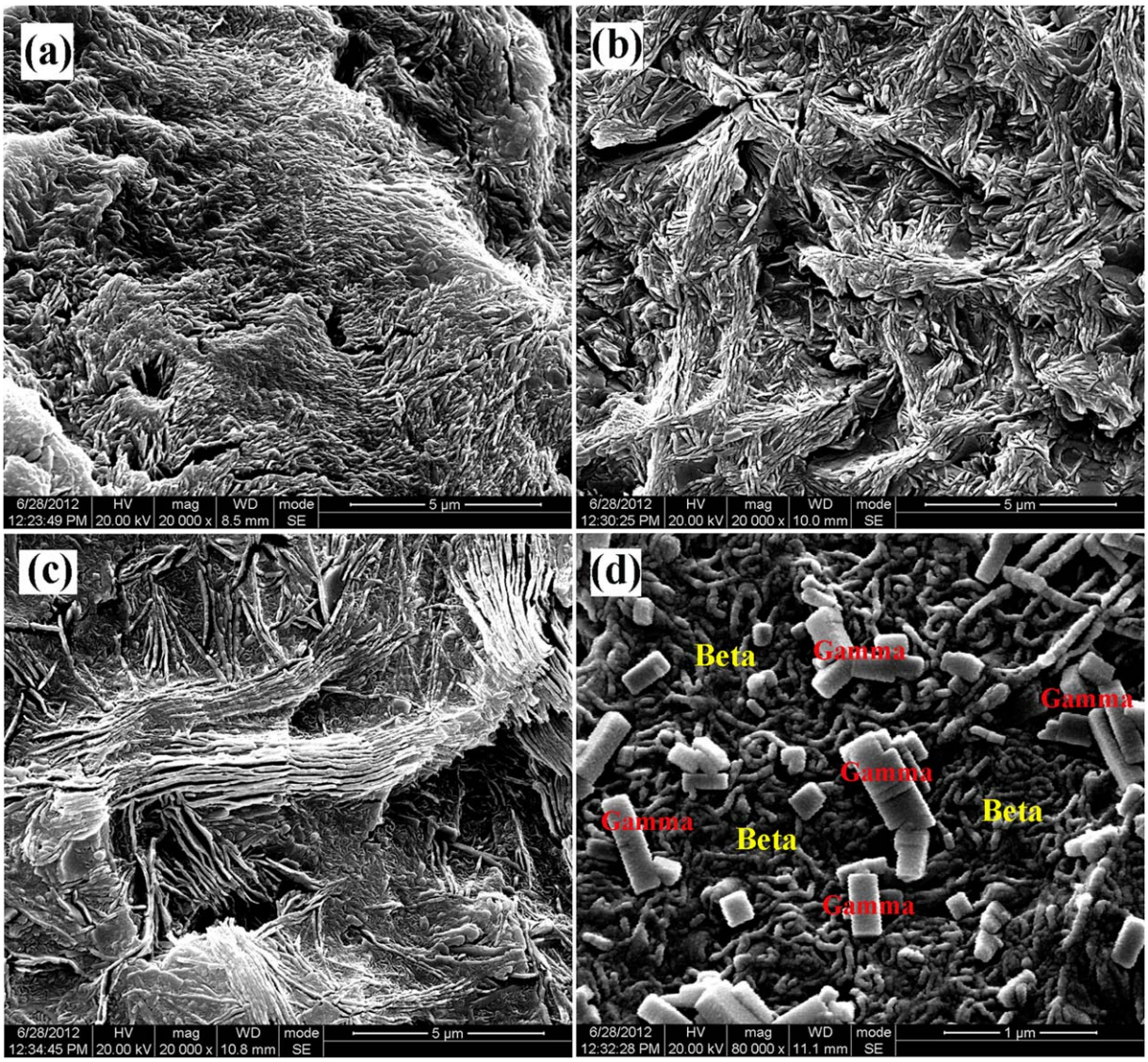

Figure 9. Secondary electron images of the etched fracture surfaces of C70/PVDF (1/99, wt/wt) composite samples, crystallized at different pressure, 260°C for 30 min: (a) 600 MPa; (b) 400 MPa; (c,d) 300 MPa. [Color figure can be viewed in the online issue, which is available at wileyonlinelibrary.com.]

of different phase transitions to pressure is different.[42] Especially, with the introduction of C70, pressure may shift the phase equilibrium, and bring a new axis to the self-assembly space. This finally resulted in the formation of polymeric nanowires under specific experimental conditions.

In addition to the C70-induced growth of nanowire arrays, bulk crystallization of PVDF occurred simultaneously at high pressure. It is known that a metastable hexagonal phase was promoted when PVDF was crystallized at high pressure and temperature.[29,30] This phase is a disordered phase, in which gauche sequences are introduced in all-trans chains, with interchain distance expanded about 10% larger than the original orthorhombic phase.[29,30] The gauche and trans sequences in this phase are not static but are interchanged dynamically in the crystalline chains,[29,30] just as in the high-pressure phase of polyethylene.[52] The hexagonal phase, which appears only at high pressures and high temperatures, is crucial to the formation of PVDF extended-chain crystals with β- or γ-form.[29,30] In this phase, molecular chains can slide very easily along the direction of chain axes as in a liquid crystal,[29,30] and lamellar thickening through the sliding diffusion below the triple point, at which the orthorhombic, hexagonal, and liquid phase coexist,[29,30] resulted in the formation of orthorhombic extended-chain PVDF crystals (β- or γ-form) with different characteristics, as shown in Figures 7–9.

Compared to conventional as-drawn PVDF, PVDF, and its copolymers with well-developed thick extended-chain lamellar crystals has stronger piezoelectric effects, as suggested by the previous investigations by Ohigashi et al.[29,30] Since thick lamellar crystals of β- or γ-form PVDF cannot be grown at ordinary

Applied Polymer SCIENCE

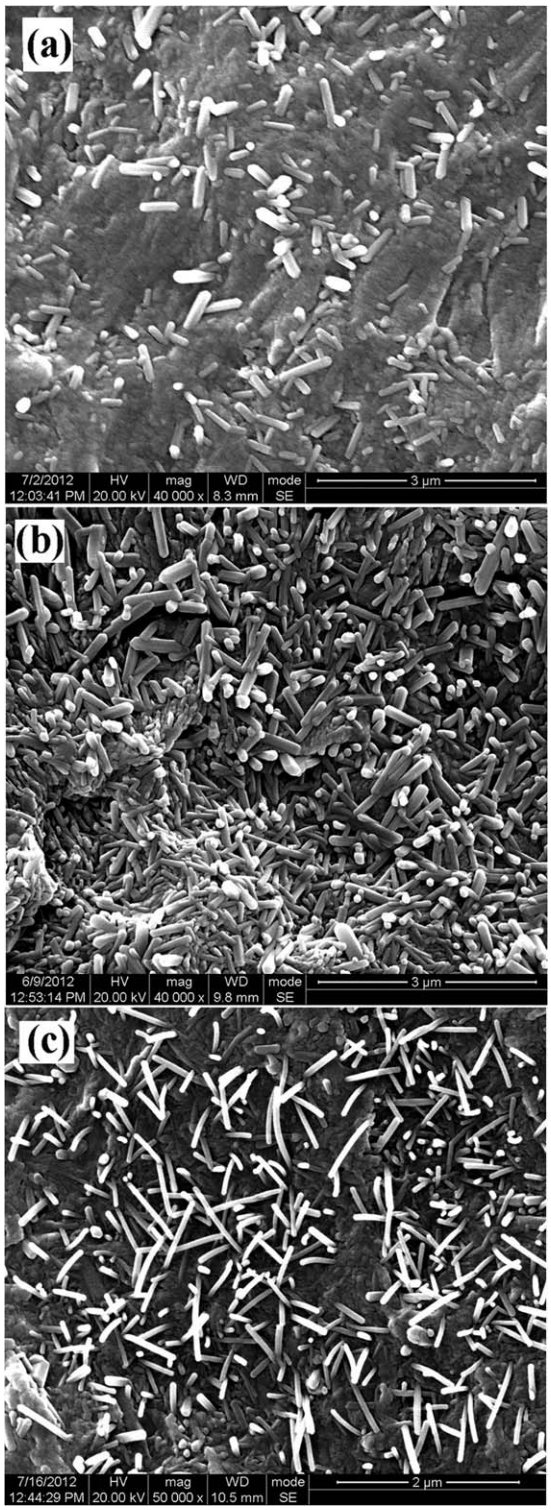

Figure 10. Secondary electron images of the etched fracture surfaces of C70/PVDF (1/99, wt/wt) composite samples, crystallized at: (a) 500 MPa and 280°C maximum quenching temperature; (b) 500 MPa, 260°C for 10 min; (c) 300 MPa, 260°C for 10 min.

pressure because of the absence of the hexagonal phase, high-pressure crystallization is necessary for the improvement of the piezoelectric properties of the binary C70/PVDF based composites.[29,30]

CONCLUSIONS

In conclusion, the effect of pressure on well-dispersed binary C70/PVDF based composites was investigated. Polymeric crystalline structures totally with extended-chain piezoelectric β- or γ-form lamellae were achieved in the composite samples by varying temperature, pressure, crystallization time, and composite composition. The *c*-axis thickness of the extended-chain β-form lamellae in the composites increased with both crystallization temperature and crystallization time, and it decreased with the increase of the applied pressure. C70 was found to be negative in the rapid formation of both β- and γ-form PVDF crystals. However, it played a crucial role in the growth of a β-form PVDF nanowire with extended-chain crystalline substructures. The template-free formation of the piezoelectric nanowires was attributed to a C70-induced self-assembly of the polymer, driven by physical interactions at high pressure. We believe the as-fabricated C70/PVDF composites, self-reinforced with unique one-dimensional piezoelectric structures, may diversify niche applications in organic-based electronic devices that require high-quality organic memory compatible with other devices, including light-emitting diodes, solar cells, transistors, and so on. The associated piezoelectric properties of the as formed composites, as well as their applications in piezoelectric devices, will be further researched and then addressed in a follow-up article.

ACKNOWLEDGMENTS

This study was supported by the National Natural Science Foundation of China (No. 50973089), the Fundamental Research Funds for the Central Universities (No. SWJTU11CX056 and SWJTU11ZT10), and State Key Laboratory of Molecular Engineering of Polymers (Fudan University; No. K2012-08). The authors extended their gratitude to Dr. Yajiang Huang (Sichuan University) for valuable discussions.

REFERENCES

1. Kratschmer, W.; Lamb, L. D.; Fostiropoulos, K.; Huffman, D. R. *Nature* **1990**, *347*, 354.
2. Giacalone, F.; Martín, N. *Adv. Mater.* **2010**, *22*, 4220.
3. Sariciftci, N. S.; Smilowitz, L.; Heeger, A. J.; Wudl, F. *Science* **1992**, *258*, 1474.
4. Tang, B. Z.; Peng, H.; Leung, S. M.; Au, C. F.; Poon, W. H.; Chen, H. L.; Wu, X. Z.; Fok, M. W.; Yu, N. T.; Hiraoka, H.; Song, C. Y.; Fu, J. S.; Ge, W. K.; Wong, G. K. L.; Monde, T.; Nemoto, F.; Su, K. C. *Macromolecules* **1998**, *31*, 103.
5. Lu, G.; Li, L.; Yang, X. *Small* **2008**, *5*, 601.
6. Rajagopalan, M.;Oh, I. K. *ACS Nano* **2011**, *5*, 2248.
7. Schon, J. H.; Kloc, C.; Siegrist, T.; Steigerwald, M.; Svensson, C.; Batlogg, B. *Nature* **2001**, *413*, 831.
8. Arora, G.; Klauda, J. B.; Sandler, S. I. *J. Phys. Chem. B* **2005**, *109*, 17267.
9. Pfuetzner, S.; Meiss, J.; Petrich, A.; Riede, M.; Leo, K. *Appl. Phys. Lett.* **2009**, *94*, 223307.

10. Cai, R. F.; Bai, X.; Chen, Y.; Huang, Z. E. *Eur. Polym. J.* **1998**, *34*, 7.
11. Higuchi, A.; Agatsuma, T.; Uemiya, S.; Kojima, T.; Mizoguchi, K.; Pinnau, I.; Nagai, K.; Freeman, B. D. *J. Appl. Polym. Sci.* **2000**, *77*, 529.
12. Tarassova, E.; Aseyev, V.; Filippov, A.; Tenhu, H. *Polymer* **2007**, *48*, 4503.
13. Zuev, V. V.; Ivanova, Y. G. *Polym. Eng. Sci.* **2012**, *52*, 1206.
14. Sun, Y. P.; Cui, C. H.; Wang, H. Q.; Li, Y. F. *Adv. Energy Mater.* **2011**, *1*, 1058.
15. Fan, X.; Cui, C. H.; Fang, G. J.; Wang, J. Z.; Li, S. Z.; Cheng, F.; Long, H.; Li, Y. F. *Adv. Funct. Mater.* **2012**, *22*, 585.
16. Meng, X. Y.; Zhang, W. Q.; Tan, Z. A.; Li, Y. F.; Ma, Y. H.; Wang, T. S.; Jiang, L.; Shu, C. Y.; Wang, C. R. *Adv. Funct. Mater.* **2012**, *22*, 2187.
17. Kang, S. J.; Park, Y. J.; Hwang, J.; Jeong, H. J.; Lee, J. S.; Kim, K. J.; Kim, H. C.; Huh, J.; Park, C. *Adv. Mater.* **2007**, *19*, 581.
18. García-Gutiérrez, M. C.; Linares, A.; Hernández, J. J.; Rueda, D. R.; Ezquerra, T. A.; Poza, P.; Davies, R. J. *Nano Lett.* **2010**, *10*, 1472.
19. Cha, S. N.; Kim, S. M.; Kim, H. J.; Ku, J. Y.; Sohn, J. I.; Park, Y. J.; Song, B. G.; Jung, M. H.; Lee, E. K.; Choi, B. L.; Park, J. J.; Wang, Z. L.; Kim, J. M.; Kim, K. *Nano Lett.* **2011**, *11*, 5142.
20. Lu, J.; Kim, S. G.; Lee, S.; Oh, I. K. *Adv. Funct. Mater.* **2008**, *18*, 1290.
21. Liu, W. D.; Zhang, Y. H.; Fang, L. F.; Zhu, B. K.; Zhu, L. P. *Chinese J. Polym. Sci.* **2012**, *30*, 568.
22. Ameduri, B. *Chem. Rev.* **2009**, *109*, 6632.
23. Li, J. J.; Meng, Q. J.; Li, W. J.; Zhang, Z. C. *J. Appl. Polym. Sci.* **2011**, *122*, 1659.
24. Wang, T. C.; Li, H. H.; Yan, S. K. *Chinese J. Polym. Sci.* **2012**, *30*, 269.
25. Zhang, Y. Y.; Jiang, S. L.; Yu, Y.; Xiong, G.; Zhang, Q. F.; Guang, G. Z. *J. Appl. Polym. Sci.* **2012**, *123*, 2595.
26. Zhang, Y. Y.; Jiang, S. L.; Yu, Y.; Zeng, Y. K.; Zhang, G. Z.; Zhang, Q. F.; He, J. G. *J. Appl. Polym. Sci.* **2012**, *125*, E314.
27. Gonzalez-Leon, J. A.; Acar, M. H.; Ryu, S.W.; Ruzette, A. V. G.; Mayes, A. M. *Nature* **2003**, *426*, 424.
28. Ryu, D. Y.; Lee, D. J.; Kim, J. K.; Lavery, K. A.; Russell, T. P. *Phys. Rev. Lett.* **2003**, *90*, 235501.
29. Hattori, T.; Kanaoka, M.; Ohigashi, H. *J. Appl. Phys.* **1996**, *79*, 2016.
30. Hattori, T.; Hikosaka, M.; Ohigashi, H. *Polymer* **1996**, *37*, 85.
31. Xi, D. K.; Huang, W. J.; Li, Z. P.; Lu, J.; Chen, X. L.; Zhou, Z. W. *Mater. Lett.* **2012**, *81*, 189.
32. Tian, J. J.; Liu, G. D.; Chen, X.; Lu, J.; Zhou, Z. W.; Huang, R. *J. Appl. Polym. Sci.* to appear. DOI: 10.1002/APP.38822.
33. Vaughan, A. S. *J. Mater. Sci.* **1993**, *28*, 1805.
34. Buonomenna, M. G.; Macchi, P.; Davoli, M.; Drioli, E. *Eur. Polym. J.* **2007**, *43*, 1557.
35. Ince-Gunduz, B. S.; Alpern, R.; Amare, D.; Crawford, J.; Dolan, B.; Jones, S.; Kobylarz, R.; Reveley, M.; Cebe, P. *Polymer* **2010**, *51*, 1485.
36. Ramasundaram, S.; Yoon, S.; Kim, K. J.; Park, C. *J. Polym. Sci. Pol. Phys.* **2008**, *46*, 2173.
37. Kang, S. J.; Park, Y. J.; Bae, I.; Kim, K. J.; Kim, H. C.; Bauer, S.; Thomas, E. L.; Park, C. *Adv. Funct. Mater.* **2009**, *19*, 2812.
38. Shah, D.; Maiti, P.; Gunn, E.; Schmidt, D. F.; Jiang, D. D.; Batt, C. A.; Giannelis, E. P. *Adv. Mater.* **2004**, *16*, 1173.
39. Dillon, D. R.; Tenneti, K. K.; Li, C. Y.; Ko, F. K.; Sics, I.; Hsiao, B. S. *Polymer* **2006**, *47*, 1678.
40. Lee, J. S.; Kim, K. J. *Fiber Polym.* **2007**, *8*, 335.
41. Wunderlich, B.; Melillo, L. *Science* **1966**, *154*, 1329.
42. Lu, J.; Huang, R.; Li, L. B.; Luo, J. B. *Macromol. Rapid Commun.* **2005**, *26*, 1478.
43. Zhang, D. P.; Tian, P. F.; Chen, X.; Lu, J.; Zhou, Z. W.; Fan, X. M.; Huang, R. *Compos. Sci. Technol.* **2013**, *77*, 29.
44. Steinhart, M.; Senz, S.; Wehrspohn, R. B.; Gösele, U.; Wendorff, J. H. *Macromolecules* **2003**, *36*, 3646.
45. Steinhart, M.; Göring, P.; Dernaika, H.; Prabhukaran, M.; Gösele, U.; Hempel, E.; Thurn-Albrecht, T. *Phys. Rev. Lett.* **2006**, *97*, 027801.
46. Wang, Z. L.; Song, J. *Science* **2006**, *163*, 242.
47. Jian, P.; Zhou, J. J.; Fang, H. F.; Wang, C. Y.; Wang, Z. L.; Xie, S. S. *Adv. Funct. Mater.* **2007**, *17*, 1303.
48. Yang, R. S.; Wang, Z. L. *Philos. Mag.* **2007**, *87*, 2097.
49. Wang, Z. L. *J. Mater. Chem.* **2005**, *15*, 1021.
50. García-Gutiérrez, M. C.; Nogales, A.; Rueda, D. R.; Domingo, C.; García-Ramos, J. V.; Broza, G.; Roslaniec, Z.; Schulte, K.; Davies, R. J.; Ezquerra, T. A. *Polymer* **2006**, *47*, 341.
51. Hernández, J. J.; García-Gutiérrez, M. C.; Rueda, D. R.; Ezquerra, T. A.; Davies, R. J. *Compos. Sci. Technol.* **2012**, *72*, 421.
52. Keller, A.; Goldbeck-Wood, G.; Hikosaka, M. *Faraday Discuss.* **1993**, *95*, 109.